

# UC Santa Barbara

## UC Santa Barbara Previously Published Works

### Title

High thermoelectric performance by resonant dopant indium in nanostructured SnTe

### Permalink

<https://escholarship.org/uc/item/1xm5199d>

### Journal

Proceedings of the National Academy of Sciences of the United States of America, 110(33)

### ISSN

0027-8424

### Authors

Zhang, Qian  
Liao, Bolin  
Lan, Yucheng  
et al.

### Publication Date

2013-08-13

### DOI

10.1073/pnas.1305735110

Peer reviewed

# High thermoelectric performance by resonant dopant indium in nanostructured SnTe

Qian Zhang<sup>a</sup>, Bolin Liao<sup>b</sup>, Yucheng Lan<sup>a</sup>, Kevin Lukas<sup>c</sup>, Weishu Liu<sup>a</sup>, Keivan Esfarjani<sup>b</sup>, Cyril Opeil<sup>c</sup>, David Broido<sup>c</sup>, Gang Chen<sup>b,1</sup>, and Zhifeng Ren<sup>a,1</sup>

<sup>a</sup>Department of Physics and Texas Center for Superconductivity, University of Houston, Houston, TX 77204; <sup>b</sup>Department of Mechanical Engineering, Massachusetts Institute of Technology, Cambridge, MA 02139; and <sup>c</sup>Department of Physics, Boston College, Chestnut Hill, MA 02467

Edited\* by Ching-Wu Chu, University of Houston, Houston, TX, and approved July 5, 2013 (received for review March 25, 2013)

From an environmental perspective, lead-free SnTe would be preferable for solid-state waste heat recovery if its thermoelectric figure-of-merit could be brought close to that of the lead-containing chalcogenides. In this work, we studied the thermoelectric properties of nanostructured SnTe with different dopants, and found indium-doped SnTe showed extraordinarily large Seebeck coefficients that cannot be explained properly by the conventional two-valence band model. We attributed this enhancement of Seebeck coefficients to resonant levels created by the indium impurities inside the valence band, supported by the first-principles simulations. This, together with the lower thermal conductivity resulting from the decreased grain size by ball milling and hot pressing, improved both the peak and average nondimensional figure-of-merit ( $ZT$ ) significantly. A peak  $ZT$  of  $\sim 1.1$  was obtained in 0.25 atom % In-doped SnTe at about 873 K.

Good thermoelectric (TE) materials should not only have high figure-of-merit ( $Z$ ), but also be environmentally friendly and cost-effective (1–5). The nondimensional figure-of-merit ( $ZT$ ) is defined as  $ZT = [S^2\sigma/(\kappa_L + \kappa_e)]T$ , where  $S$  is the Seebeck coefficient,  $\sigma$  the electrical conductivity,  $\kappa_L$  the lattice thermal conductivity,  $\kappa_e$  the electronic thermal conductivity, and  $T$  the absolute temperature. Lead chalcogenides and their alloys can be engineered to exhibit high  $ZT$ s; however, environmental concern regarding Pb prevents their deployment in large-scale applications (6–10). Tin telluride (SnTe), a lead-free IV–VI narrow band-gap semiconductor has not been considered favorably as a good thermoelectric material because of its low  $ZT$  due to the relatively low Seebeck coefficient and high electronic thermal conductivity caused by intrinsic Sn vacancies (11–13), although SnTe has been used to alloy with other tellurides for better TE properties (14–26). Even though there has been no real success in achieving good TE properties of lead-free SnTe, the similarity between the electronic band structure of SnTe and that of PbTe and PbSe (27–31) suggests it has the potential to be a good TE material, especially given the two valence bands (light-hole and heavy-hole bands) that contribute to the hole density of states. The main difficulty here, however, is the fact that the separation between the light-hole and heavy-hole band edges in SnTe is estimated to be in the range of  $\sim 0.3$  to  $\sim 0.4$  eV (27, 29), larger than those of PbTe or PbSe (9), rendering the benefit of the heavier mass for the Seebeck coefficient less significant.

In this paper, we prepared In-doped SnTe by high-energy ball milling and hot pressing and measured the samples up to 873 K without experiencing any mechanical strength issues. We show, based on both experiments and first-principles simulation, that a small amount of In-doping helps create resonant states around the Fermi level inside the valence band, which increases the Seebeck coefficient, especially at room temperature, leading to improvements in both average  $ZT$  and peak  $ZT$ , combined with the decreased lattice thermal conductivity due to the increased density of grain boundaries (32–34). Peak  $ZT$  value reaches  $\sim 1.1$  at about 873 K for SnTe doped with 0.25 atom % In.

Single-phased In-doped SnTe was obtained by ball milling and hot pressing. Fig. 1 presents the X-ray diffraction (XRD) patterns of  $\text{In}_x\text{Sn}_{1-x}\text{Te}$  ( $x = 0, 0.0025, 0.005, \text{ and } 0.01$ ). All the peaks can be indexed to the face-centered structure (space group  $\text{Fm}\bar{3}\text{m}$ ). No impurity phase was found, despite the increasing content of In. First-principles calculations (Table S1) indicated it is energetically favorable for In to substitute for Sn, which is consistent with the case in In-doped PbTe and PbSe. In previous work, we found In substitutes for Pb in PbTe and PbSe, which is the same with In-doped SnTe, but it is n-type doping in  $\text{In}_x\text{Pb}_{1-x}\text{Te}$  and  $\text{In}_x\text{Pb}_{1-x}\text{Se}$ , which is different from p-type doping by In in SnTe, as we are reporting in this work (35, 36).

The electrical conductivities decrease with increasing temperature, as shown in Fig. 2A, showing the typical behavior of degenerate semiconductors. With increasing content of In, the electrical conductivity decreases, especially at room temperature, from  $\sim 7 \times 10^5 \text{ S}\cdot\text{m}^{-1}$  to  $\sim 2 \times 10^5 \text{ S}\cdot\text{m}^{-1}$ . The hole concentration indicated by the Hall measurement, however, changes in an interesting way with increasing In content: it drops below the intrinsic value at the beginning and starts to rise after  $x \geq 0.0025$  (as shown in Fig. 3A). Based on this observation, we conclude In atoms should be p-type dopants and explain the change of the carrier concentration as follows. The intrinsic SnTe is p-type because of the Sn vacancies (19). Those vacancies create empty electronic states and behave like p-type dopants. If we dope SnTe with In, In atoms first fill the Sn vacancies. Despite being p-type dopants, they are not as “strong” as the vacancies, in the sense that they induce fewer holes (examined by the simulation shown in Table S1); thus, at low doping levels, the p-type charge concentration decreases. However, as the doping level is increased, at some point all the Sn vacancies are filled with In, and beyond that point, excessive In atoms substitute for Sn, and the p-type charge concentration increases again (Fig. 3A). However, when In is more than the solubility limit in SnTe, the extra In atoms act as donors, which decreases the hole carrier concentration ( $x = 0.01$ ) (37). The fact that the electrical conductivity decreases all the way indicates that the In dopants affected the hole mobility significantly (shown in Fig. 3B), as the result of both increased effective mass and impurity scattering. The Seebeck coefficients increase with temperature in the whole temperature range and also increase with In content, as shown in Fig. 2B. No bipolar effect is evident, even up to 873 K, in all the compositions despite the small band gap  $\sim 0.18$  eV for SnTe (29, 31). All the measured Seebeck coefficients are positive, consistent with the density of states (DOS) calculation presented in

Author contributions: Q.Z. designed research; Q.Z., B.L., Y.L., K.L., W.L., K.E., C.O., and D.B. performed research; Q.Z., B.L., Y.L., D.B., G.C., and Z.R. analyzed data; and Q.Z., B.L., Y.L., D.B., G.C., and Z.R. wrote the paper.

The authors declare no conflict of interest.

\*This Direct Submission article had a prearranged editor.

<sup>1</sup>To whom correspondence may be addressed. E-mail: zren@uh.edu or gchen2@mit.edu.

This article contains supporting information online at [www.pnas.org/lookup/suppl/doi:10.1073/pnas.1305735110/-DCSupplemental](http://www.pnas.org/lookup/suppl/doi:10.1073/pnas.1305735110/-DCSupplemental).

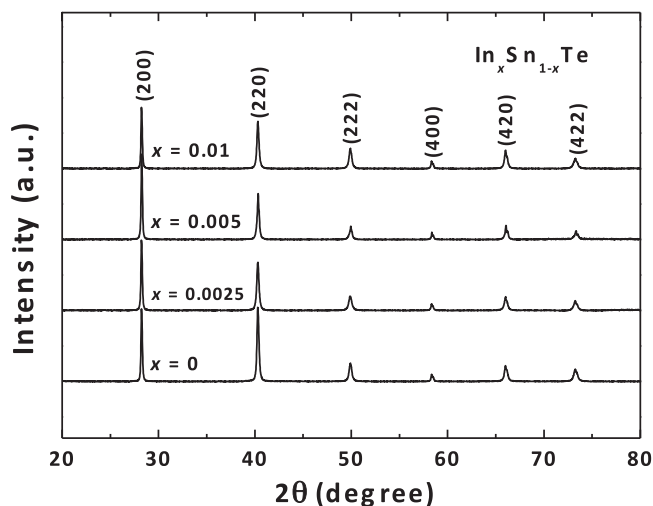


Fig. 1. XRD patterns for  $\text{In}_x\text{Sn}_{1-x}\text{Te}$  ( $x = 0, 0.0025, 0.005, \text{ and } 0.01$ ) prepared by ball milling and hot pressing.

Fig. 4 and different from In-doped PbTe and PbSe, in which In turned out to be an n-type dopant (36, 38). Fig. 2C shows the power factor for undoped and In-doped SnTe. The highest power factor reaches  $\sim 2.0 \times 10^{-3} \text{ W}\cdot\text{m}^{-1}\cdot\text{K}^{-2}$  at about 873 K, higher than all the reported power factors of doped PbTe and PbSe at this temperature (9, 39–41). Most importantly, the average power factor is increased a great deal by In doping. Compared with the undoped SnTe prepared by melting and hand milling (M+HM) (broken line), the electrical properties of the ball-milled samples are not different.

Fig. 5 shows variation of the Seebeck coefficient vs. carrier concentration for both pure SnTe and In-doped SnTe. The Seebeck coefficients of undoped SnTe with different hole concentrations ( $2 \times 10^{20}$  to  $1.8 \times 10^{21} \text{ cm}^{-3}$ ) were obtained previously by annealing under different conditions (open circles) (27). The carrier concentration obtained in this work is  $\sim 2.35 \times 10^{20} \text{ cm}^{-3}$  (filled circle). Unlike PbTe and PbSe (7, 9, 36, 39, 40), the Seebeck coefficient of SnTe shows abnormal variation with increasing carrier concentration, which was qualitatively explained previously by two parabolic band models (27) and density functional theory (DFT) calculations (31). The valence band model (VBM), which takes into account the nonparabolicity of the light-hole band (solid line), provides a quantitative fit to all the Seebeck coefficient data, except for those of In-doped samples, and thus is expected to best depict the contribution from the intrinsic band structure of SnTe (29). The model details for TE transport of p-type SnTe may be found in *SI Text*. Compared with the same model we used for PbTe and PbSe (9, 36), two major differences should be stated. The L point energy gap,  $E_g$ , is smaller for SnTe, making the nonparabolicity larger. This makes the Seebeck coefficient drop faster with increasing concentration, as seen in Fig. S1. The light-hole–heavy-hole band edge energy difference is 0.12 eV for PbTe, 0.26 eV for PbSe, and 0.35 eV for SnTe (9, 29, 36); thus, the heavy-hole contribution is relatively weaker for SnTe. This may be seen from the fact that there is not much difference between the predictions of VBM and those of the two-band Kane model (which ignores the heavy-hole band contribution) at room temperature for SnTe, until  $10 \times 10^{19} \text{ cm}^{-3}$ . However, the contribution from the heavy-hole band gradually increases at higher temperatures (Fig. S2) as for PbSe (9, 36), helping improve the Seebeck coefficient at high temperature and suppress the bipolar effect. Although the Seebeck coefficients of bismuth- (Bi-) and Cu-doped samples agree well with the VBM model, as shown in Fig. 5, indicating

pure doping effects, the deviation of the In-doped samples from the VBM model implies that there must be mechanisms through which In dopants significantly alter the band structure of pure SnTe near the band edge. One of the possible mechanisms is the introduction of resonant levels (6, 42–44) into the valence band. Fig. 4 shows the DOS of pure SnTe, Bi-doped SnTe, and In-doped SnTe near the top of the valence band. A well-defined peak is observed in the DOS of In-doped SnTe that may contribute to the large deviation of the Seebeck coefficient from the VBM model. One may question whether the observed features are a result of the limited size of the supercell and thus the artificial interactions between In atoms. Similar features, however, are not observed in Bi-doped SnTe with the same supercell size. Therefore, we believe the added feature originates from the interactions of the In atoms with the host atoms. Because of the limitation of computing resources, a sufficiently dense k-mesh for calculating transport properties for the supercells is not possible at this stage; also, the simulated supercells are too small

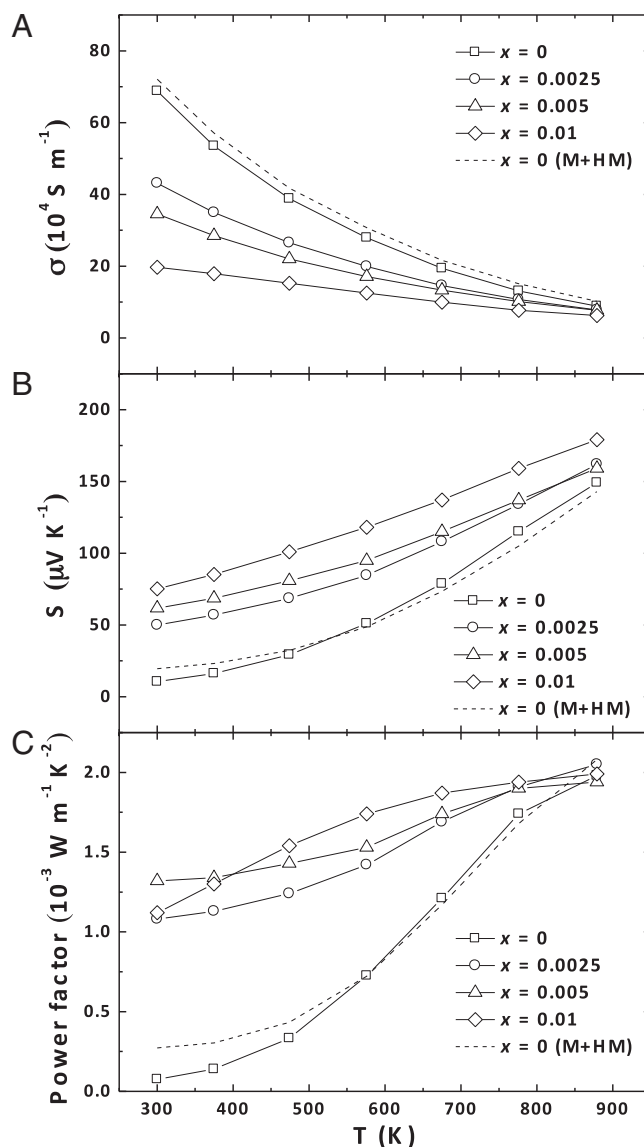
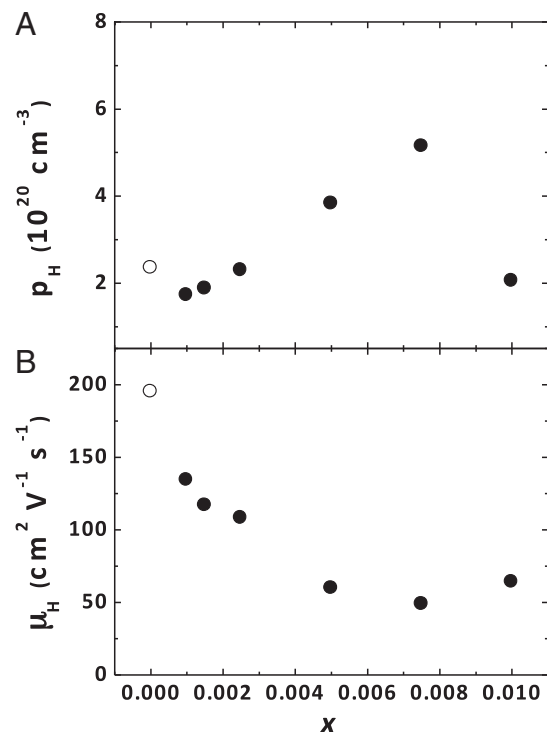
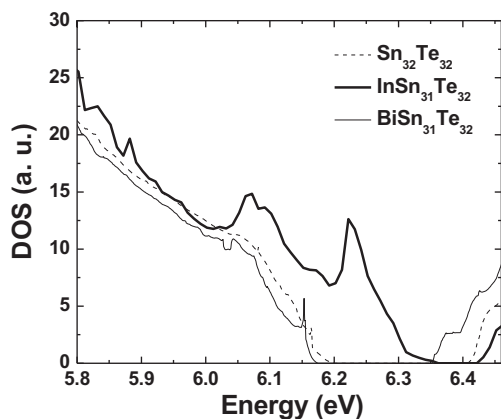


Fig. 2. Temperature dependence of (A) electrical conductivity, (B) the Seebeck coefficient, and (C) the power factor for  $\text{In}_x\text{Sn}_{1-x}\text{Te}$  ( $x = 0, 0.0025, 0.005, \text{ and } 0.01$ ). The undoped SnTe prepared by melting, hand milling, and hot pressing (M+HM) is shown for comparison (broken line).



**Fig. 3.** Hall carrier concentration (A) and Hall mobility (B) at room temperature with respect to the doping content  $x$ .  $\circ$ , undoped SnTe;  $\bullet$ , In-doped SnTe.

to represent a realistic doping concentration. [The simulated supercell corresponds to 3% In concentration, with a Fermi level located slightly below the DOS “hump.” With the doping concentration achieved in the experiments, the Fermi level is expected to reside close to the DOS peak. An alternative simulation method, such as a Korringa–Kohn–Rostoker coherent-potential-approximation (KKR-CPA) calculation (44), is required in cases of more dilute doping concentrations.] Thus, a direct evaluation of the effect of the features in DOS on the Seebeck coefficient is not



**Fig. 4.** Comparison of DOS for undoped SnTe (broken line), Bi-doped SnTe (solid line), and In-doped SnTe (bold solid line). Sharp features are observed in the DOS of In-doped SnTe near the band edge, to which the abnormal Seebeck coefficient might be attributed. The simulated supercell configuration corresponds to 3 atom % In concentration, which is higher than that achieved in the experiment. The Fermi level in the simulation resides at 6.207 eV, slightly below the DOS hump. With the experimental In concentration, the Fermi level is expected to sit around the DOS peak.

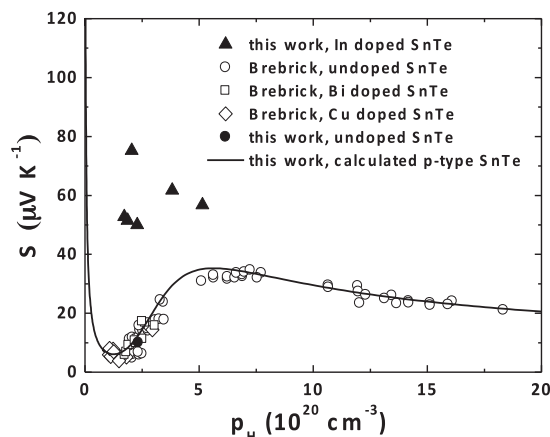


**Fig. 5.** Room temperature Pisarenko plot for ball-milled and hot-pressed  $\text{In}_x\text{Sn}_{1-x}\text{Te}$  ( $x = 0$ , shown by  $\bullet$ ;  $x = 0.001, 0.0015, 0.0025, 0.005, 0.0075$ , and  $0.01$ , shown by  $\blacktriangle$ ) in comparison with reported data on undoped SnTe ( $\circ$ ), Bi-doped SnTe ( $\square$ ), and Cu-doped SnTe ( $\diamond$ ) by Brebrick and Strauss (27). The solid curve is based on the VBM (light nonparabolic band and heavy parabolic band) with the heavy-hole effective mass of SnTe  $m^*/m_e = 1.92$ .

available for now. However, the rich features introduced by In atoms are speculated to play an important role in the enhanced TE properties.

The other problem we should resolve is the high thermal conductivity induced by intrinsic Sn vacancies, causing very high electrical conductivity. By In doping, the decreased electrical conductivity results in a reduced electronic part of the thermal conductivity determined by the Wiedemann–Franz law ( $\kappa_c = L\sigma T$ ), where  $L$  is the Lorenz number. The Lorenz number is calculated using the VBM in a way similar to that of the Seebeck coefficient, including contributions from both nonparabolic light-hole and parabolic heavy-hole bands. The detailed expressions used are included in *SI Text*. Fig. 6A–C gives the temperature dependences of the thermal diffusivity, specific heat, total thermal conductivity, and lattice thermal conductivity (obtained by subtracting the electronic contribution from the total thermal conductivity) of the undoped and In-doped SnTe, respectively. With increasing temperature, the total thermal conductivity decreases rapidly without showing any bipolar effect, consistent with the behavior of the Seebeck coefficient in Fig. 2B. The total thermal conductivities of all In-doped SnTe are lower than the undoped sample. Compared with the undoped SnTe prepared by melting and hot pressing (dotted line), the samples prepared by ball milling and hot pressing exhibit lower lattice thermal conductivity, which may be attributed to the increased density of grain boundaries by ball milling. In Fig. 7, the representative microstructure of ball-milled and hot-pressed In-doped SnTe is presented. Scanning electron microscopic (SEM) images shown in Fig. 7A indicate that the  $\text{In}_{0.0025}\text{Sn}_{0.9975}\text{Te}$  samples consist of both big grains with diameters of several tens of microns and small grains. The observed small cavities may contribute to the lower lattice thermal conductivity. The densities of all the samples are listed in Table S2. The size of the small grains is about 1  $\mu\text{m}$ , as shown in Fig. 7B, less than one tenth that of the big grains. Nanograins in the samples also are observed via transmission electron microscopy (TEM). Fig. 7C shows a typical bright-field TEM image of the nanograins, with sizes around 100 nm. As a result, the lattice thermal conductivity of the samples is greatly reduced by significantly enhanced boundary scatterings of the phonons, as shown in Fig. 6C. Selected area electron diffraction and high-resolution TEM (HRTEM) images show that all the grains, whether in microns or nanometers, are single crystals with clean boundaries and good crystallinity, as shown in

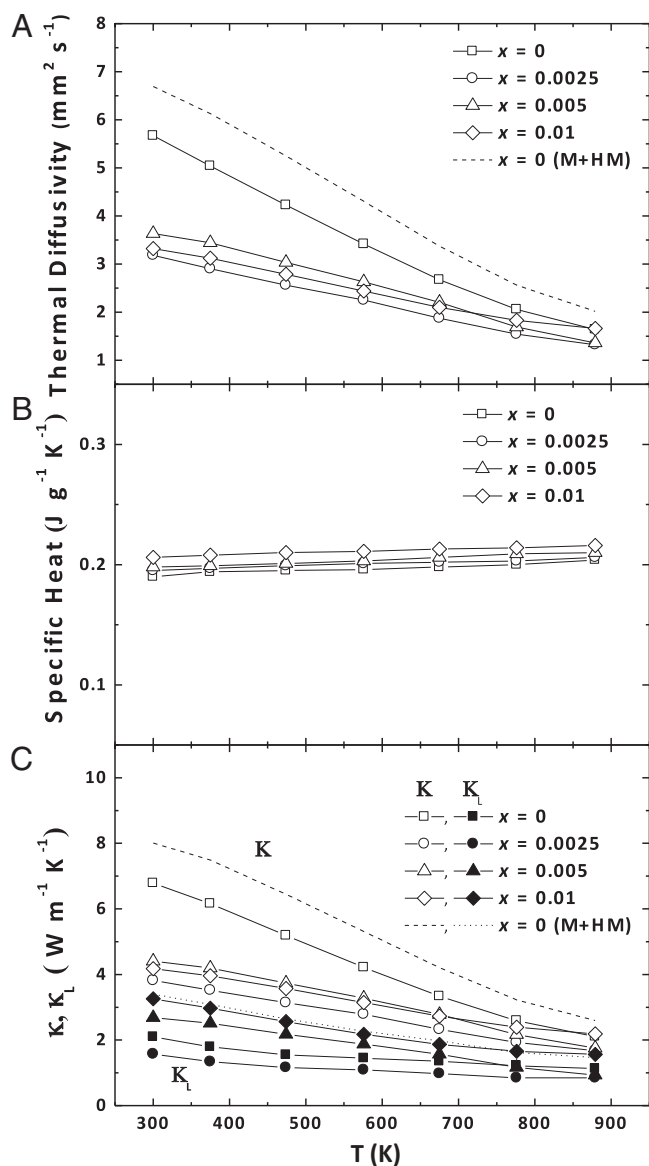


**Fig. 6.** Temperature dependence of (A) thermal diffusivity (the undoped SnTe prepared by melting and hot pressing is shown by the broken line), (B) specific heat (the specific heat of sample  $x = 0$  is used for the undoped SnTe prepared by melting and hot pressing), and (C) total thermal conductivity and lattice thermal conductivity for  $\text{In}_x\text{Sn}_{1-x}\text{Te}$  ( $x = 0, 0.0025, 0.005$ , and  $0.01$ ) (the undoped SnTe prepared by melting and hot pressing is shown by the broken line).

Fig. 7D. The crystalline grains and boundaries would benefit the transport of charge carriers, as observed in nanograned  $\text{Bi}_x\text{Sb}_{2-x}\text{Te}_3$  bulks (45), without degrading the electronic properties (Fig. 2).

Fig. 8 summarizes the  $ZT$  values of different samples. The two intrinsic valence bands contribute to the peak  $ZT$  value  $\sim 0.7$  at about 873 K for the undoped SnTe. The decreased lattice thermal conductivity by ball milling further boosts the peak  $ZT$  value to  $\sim 0.8$ . However, the  $ZT$  values in both cases are quite low, below 600 K, resulting in low average  $ZT$ s. The enhanced Seebeck coefficient by resonant states increased both the peak and average  $ZT$ s in the In-doped nanostructured SnTe. A peak  $ZT \sim 1.1$  is obtained at about 873 K in  $\text{In}_{0.0025}\text{Sn}_{0.9975}\text{Te}$ .

In summary, nanostructured In-doped SnTe with a  $ZT > 1$  has been prepared by ball milling and hot pressing. The improved  $ZT$  (peaked around 1.1 at about 873 K in 0.25 atom % In-doped

SnTe) incorporates both the high Seebeck coefficient resulting from the two valence bands and the local resonant states around Fermi level created by In-doping and the lowered lattice thermal conductivity owing to the increased phonon interface scattering. This lead-free TE material is a potential candidate to replace lead chalcogenides used at medium to high temperatures for waste heat recovery applications. Further improvement is expected by adding suitable nanoinclusions or alloying with SnSe and SnS to decrease the thermal conductivity and increase the Seebeck coefficient.

### Synthesis

Samples with nominal compositions of  $\text{In}_x\text{Sn}_{1-x}\text{Te}$  ( $x = 0, 0.001, 0.0015, 0.0025, 0.005, 0.0075$ , and  $0.01$ ) were prepared by directly ball milling the raw materials In (powder, 99.99%), Sn (powder, 99.9%), and Te (chunks, 99.999%) in a stainless steel jar with a high-energy ball mill, SPEX 8000D (SPEX SamplePrep), and the raw materials (In, Sn, and Te) were sealed inside the jar in an argon-filled glove box. In addition to using ball milling, the undoped SnTe also was prepared by melting and cooling in a quartz tube, followed by hand milling for comparison. Samples made in such a way are labeled M+HM. The powder was loaded into the graphite die and consolidated by dc-induced hot pressing.

### Calculations

DFT-based calculations were carried out to answer the following questions: (i) whether In atoms substitute for tin or tellurium in the structure [the possibility of In atoms being interstitial was not considered here based on the fact that the interstitial impurity states generally are high-energy configurations (46)]; (ii) how In atoms are compared with Sn vacancies as p-type dopants; and (iii) what effects the In atoms have on the electronic structure, especially the DOS of the pure system near the band gap. We followed the strategy in ref. 47 and constructed supercells consisting of eight-unit cells ( $\text{Sn}_{32}\text{Te}_{32}$ ), and the total energy of two different configurations ( $\text{InSn}_{31}\text{Te}_{32}$ , and  $\text{Sn}_{32}\text{Te}_{31}\text{In}$ ) was calculated and compared (details are provided in Table S1). For comparison, we did the same supercell calculations for Bi-doped SnTe. The Quantum Espresso package (48) was used for the calculation, with norm-conserving pseudopotentials with the local

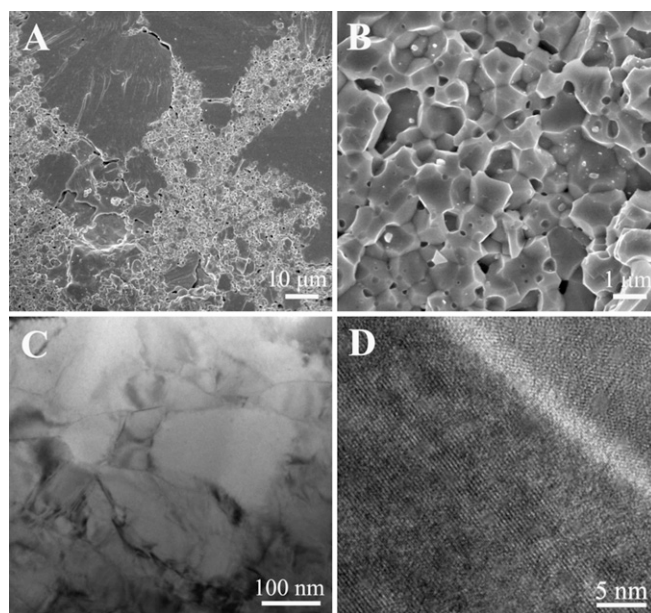


**Fig. 7.** Representative SEM (A and B), TEM (C), and HRTEM (D) images for as-prepared  $\text{In}_{0.0025}\text{Sn}_{0.9975}\text{Te}$  samples by ball milling and hot pressing.

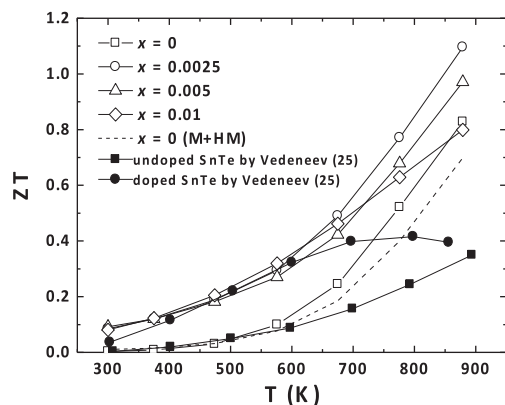


**Fig. 8.** Temperature dependence of  $ZT$  for  $\text{In}_x\text{Sn}_{1-x}\text{Te}$  ( $x = 0, 0.0025, 0.005,$  and  $0.01$ ) compared with the reported data on undoped SnTe (0.5–2.0 atom % Te excess) (■) by Vedenev et al. (25) and codoped SnTe (0.5–2.0 atom % Te excess) with 1 atom % In and 1 atom % Ag (●) by Vedenev et al. (25). The undoped SnTe prepared by melting and hot pressing is included for comparison (broken line).

density approximation functional (49). The spin–orbit interaction was taken into account, and all of supercells were fully relaxed. The cutoff energy for the plane wave basis was chosen as 60 Rydberg and a  $4 \times 4 \times 4$  k-mesh was used for the self-consistent-field (SCF) calculation, whereas a  $30 \times 30 \times 30$  mesh was used for the non-SCF and DOS calculation. The tetrahedron method was used to integrate the DOS. The simulation results are discussed in later sections.

- Rowe DM (2006) General principles and basic considerations. *CRC Handbook of Thermoelectrics, Macro to Nano*, ed Rowe DM (CRC, Boca Raton, FL), pp 1-1–1-10.
- Zhang Q, et al. (2008) High figures of merit and natural nanostructures in  $\text{Mg}_2\text{Si}_0.8\text{Sn}_0.6$  based thermoelectric materials. *Appl Phys Lett* 93(10):102109.
- Poudel B, et al. (2008) High-thermoelectric performance of nanostructured bismuth antimony telluride bulk alloys. *Science* 320(5876):634–638.
- Hochbaum AI, et al. (2008) Enhanced thermoelectric performance of rough silicon nanowires. *Nature* 451(7175):163–167.
- Zebarjadi M, Esfarjani K, Dresselhaus MS, Ren ZF, Chen G (2012) Perspectives on thermoelectrics: From fundamentals to device applications. *Energy Environ Sci* 5(1): 5147–5162.
- Heremans JP, et al. (2008) Enhancement of thermoelectric efficiency in PbTe by distortion of the electronic density of states. *Science* 321(5888):554–557.
- Pei Y, et al. (2011) Convergence of electronic bands for high performance bulk thermoelectrics. *Nature* 473(7345):66–69.
- Biswas K, et al. (2011) Strained endotaxial nanostructures with high thermoelectric figure of merit. *Nat Chem* 3(2):160–166.
- Zhang Q, et al. (2012) Heavy doping and band engineering by potassium to improve the thermoelectric figure of merit in p-type PbTe, PbSe, and PbTe(1-y)Se(y). *J Am Chem Soc* 134(24):10031–10038.
- Zhao LD, et al. (2012) Thermoelectrics with earth abundant elements: High performance p-type PbS nanostructured with SrS and CaS. *J Am Chem Soc* 134(18): 7902–7912.
- Brebrick RF (1963) Deviations from stoichiometry and electrical properties in SnTe. *J Phys Chem Solids* 24(1):27–36.
- Kafalas JA, Brebrick RF, Strauss AJ (1964) Evidence that SnTe is semiconductor. *Appl Phys Lett* 4(5):93–94.
- Rogacheva E (2012) Nonstoichiometry and properties of SnTe semiconductor phase of variable composition, stoichiometry and materials science. *When Numbers Matter*, eds Innocenti A, Kamaruzaman N (InTech, New York), pp 105–144.
- Gruzinov BF, Drabkin IA, Zakomornaya EA (1981) Electrical-properties of  $(\text{PbSe})_{1-x}(\text{SnTe})_x$  solid-solutions doped with In. *Sov Phys Semicond* 15(2):190–193.
- Androulakis J, et al. (2007) Spinodal decomposition and nucleation and growth as a means to bulk nanostructured thermoelectrics: Enhanced performance in  $\text{Pb}(1-x)\text{Sn}(x)\text{Te}$ -PbS. *J Am Chem Soc* 129(31):9780–9788.
- Arachchige IU, Kanatzidis MG (2009) Anomalous band Gap evolution from band inversion in  $\text{Pb}_{1-x}\text{Sn}_x\text{Te}$  nanocrystals. *Nano Lett* 9(4):1583–1587.
- Shi X, Salvador JR, Yang J, Wang H (2011) Prospective thermoelectric materials:  $(\text{AgSbTe}_2)_{100-x}(\text{SnTe})_x$  quaternary system ( $x = 80, 85, 90,$  and  $95$ ). *Sci Adv Mater* 3(4):667–671.
- Han MK, Androulakis J, Kim SJ, Kanatzidis MG (2012) Lead-free thermoelectrics: High figure of merit in p-type  $\text{AgSn}_m\text{SbTe}_{m+2}$ . *Adv Energy Mater* 2(1):157–161.
- Chen Y, et al. (2012) SnTe-AgSbTe<sub>2</sub> thermoelectric alloys. *Adv Energy Mater* 2(1):58–62.
- Nasirov YN, Feiziev YS (1967) Effect of small substitutions of tin by neodymium on thermoelectric properties of SnTe. *Phys Status Solidi* 24(2):K157–K159.
- Nasirov YN, Sultanova NP, Osmanov TG (1969) Thermoelectric properties of solid solutions based on SnTe-A<sup>III</sup>Te-type tin telluride. *Phys Status Solidi* 35(1):K39–K42.
- Sultanova NR, Nasirov YN, Zargarova MI, Pirzade MM (1974) Thermoelectric properties of a solid solution of the system SnTe-ZnTe. *Inorg Mater* 10(2):1219–1221.
- Rustamov PG, Alidzhanov MA, Babaev YN (1976) The system SnTe-Tl<sub>2</sub>Te<sub>3</sub>. *Inorg Mater* 12(5):715–717.
- Bushmarina GS, Gruzinov BF, Drabkin IA, Lev EY, Yunev VM (1984) Characteristics of the effects of In as a dopant in SnTe. *Sov Phys Semicond* 18(12):1374–1377.
- Vedenev VP, Krivoruchko SP, Sabo EP (1998) Tin telluride based thermoelectrical alloys. *Semicond* 32(3):241–244.
- Asadov MM, Alidzhanov MA, Mamedov FM, Kelbaliev GI (1998) Electrical conductivity and thermoelectric power of SnTe-based alloys doped with Fe. *Inorg Mater* 34(5):442–444.
- Brebrick RF, Strauss AJ (1963) Anomalous thermoelectric power as evidence for two-valence bands in SnTe. *Phys Rev* 131(1):104–110.
- Efimova BA, Kaidanov VI, Moizhes BY, Chernik IA (1966) Band model of SnTe. *Sov Phys-Sol Stat* 7(8):2032–2034.
- Rogers LM (1968) Valence band structure of SnTe. *J Phys D Appl Phys* 1(7):845–848.
- Santhanam S, Chaudhuri AK (1981) Transport-properties of SnTe interpreted by means of a 2 valence band model. *Mater Res Bull* 16(8):911–917.
- Singh DJ (2010) Thermopower of SnTe from Boltzmann transport calculations. *Funct Mater Lett* 3(4):223–226.
- Ganesan N, Sivaramakrishnan V (1988) Evidence for the domination of heavy holes and lattice scattering in SnTe from electrical transport measurements on polycrystalline thin-films. *J Phys D Appl Phys* 21(5):784–788.
- Dresselhaus MS, et al. (2007) New directions for low-dimensional thermoelectric materials. *Adv Mater* 19(8):1043–1053.
- Lan YC, Minnich AJ, Chen G, Ren ZF (2010) Enhancement of thermoelectric figure-of-merit by a bulk nanostructuring approach. *Adv Funct Mater* 20(3):357–376.
- Guch M, Sankar CR, Salvador J, Meisner G, Kleinke H (2011) Thermoelectric properties of In-doped PbTe. *Sci Adv Mater* 3(4):615–620.
- Zhang Q, et al. (2012) Study of the thermoelectric properties of lead selenide doped with boron, gallium, indium, or thallium. *J Am Chem Soc* 134(42):17731–17738.
- Pei YZ, May AF, Snyder GJ (2011) Self-tuning the carrier concentration of PbTe/Ag<sub>2</sub>Te composites with excess Ag for high thermoelectric performance. *Adv Energy Mater* 1(2):291–296.
- Xiong K, et al. (2010) Behaviour of group IIIA impurities in PbTe: Implications to improve thermoelectric efficiency. *J Phys D Appl Phys* 43(40):1–8.
- Pei Y, LaLonde A, Iwanaga S, Snyder GJ (2011) High thermoelectric figure of merit in heavy hole dominated PbTe. *Energy Environ Sci* 4(6):2085–2089.
- Wang H, Pei Y, LaLonde AD, Snyder GJ (2011) Heavily doped p-type PbSe with high thermoelectric performance: an alternative for PbTe. *Adv Mater* 23(11):1366–1370.
- Zhang QY, et al. (2012) Enhancement of thermoelectric figure-of-merit by resonant states of aluminium doping in lead selenide. *Energy Environ Sci* 5(1):5246–5251.

## Characterizations

X-ray diffraction spectra analysis was conducted on a PANalytical multipurpose diffractometer with an X'Celerator detector (PANalytical X'Pert Pro). The microstructures were investigated by an SEM (JEOL 6340F) and an HRTEM (JEOL 2010F). The electrical resistivity ( $\rho$ ) and Seebeck coefficient ( $S$ ) were measured simultaneously on a commercial system (ULVAC ZEM-3) from room temperature to 873 K, and then back to room temperature for the stability demonstration (see Figs. S3 and S4). The thermal conductivity  $\kappa$  was calculated using  $\kappa = D\alpha C_p$ , where  $D$  is the volumetric density determined by the Archimedes method,  $\alpha$  the thermal diffusivity measured on a laser flash apparatus (Netzsch LFA 457), and  $C_p$  the specific heat obtained on a differential scanning calorimetry thermal analyzer (Netzsch DSC 404 C). The Hall coefficient  $R_H$  at room temperature was measured using the Physical Properties Measurement System (Quantum Design). The Hall carrier concentration  $n_H$  and Hall mobility  $\mu_H$  were calculated using  $n_H = 1/(eR_H)$  and  $\mu_H = \sigma R_H$ . Error bars were not shown in the figures to increase the readability of the curves. The uncertainty for the electrical conductivity is 3%, the Seebeck coefficient 5%, and the thermal conductivity 7% (we include the uncertainty for the thermal diffusivity 4%, the specific heat 5%, and the density  $\sim 3\%$ ), so the combined uncertainty for the power factor is 10% and that for the  $ZT$  value is 12%.

**ACKNOWLEDGMENTS.** This work is supported by the Solid-State Solar Thermal Energy Conversion Center (S<sup>3</sup>TEC), an Energy Frontier Research Center funded by the US Department of Energy, Office of Science, Office of Basic Energy Science under Award DE-SC0001299. The computing resource is provided, in part, by the National Science Foundation through TeraGrid (Ranger).

42. Kaĭdanov VI, Nemov SA, Ravich YI (1992) Resonant scattering of carriers in IV-VI semiconductors. *Sov Phys-Semicond* 26(2):113–125.
43. Heremans JP, Wiendlocha B, Chamoire AM (2012) Resonant levels in bulk thermoelectric semiconductors. *Energ Environ Sci* 5(2):5510–5530.
44. Jaworski CM, Wiendlocha B, Jovovic V, Heremans JP (2011) Combining alloy scattering of phonons and resonant electronic levels to reach a high thermoelectric figure of merit in PbTeSe and PbTeS alloys. *Energ Environ Sci* 4(10):4155–4162.
45. Lan YC, et al. (2009) Structure study of bulk nanograined thermoelectric bismuth antimony telluride. *Nano Lett* 9(4):1419–1422.
46. Ehrhart P (1991) *Properties and Interactions of Atomic Defects in Metals and Alloys*, ed Ullmaier H (Springer, Berlin), Vol 25.
47. Ahmad S, Hoang K, Mahanti SD (2006) Ab initio study of deep defect states in narrow band-gap semiconductors: Group III impurities in PbTe. *Phys Rev Lett* 96(5):056403.
48. Giannozzi P, et al. (2009) QUANTUM ESPRESSO: A modular and open-source software project for quantum simulations of materials. *J Phys Condens Matter* 21(39):395502.
49. Perdew JP, Zunger A (1981) Self-interaction correction to density-functional approximations for many-electron systems. *Phys Rev B* 23(10):5048–5079.